Chapter 2

Modeling copper cables and PCBs

2.1. Introduction

A proper channel model is a good basis for a correct understanding of any transmission system. The goal of this chapter is to identify an accurate time-domain model with a focus on high-speed time-domain (transient) simulations. Both conductor and dielectric loss need to be modeled. We compare the model with measurements on cables and printed circuit boards (PCBs) in the time and frequency domains to be able to assess its accuracy.

Well-known textbooks [Gardiol], [Grivet], [Chipman], [Ramo] typically describe accurate models for the skin-effect magnitude and phase shift, and some also describe an analytical skin-effect step response. However, the modeling of dielectric loss at high frequencies is still a developing field and has received much attention recently. For high-speed serial links over printed circuit boards, accurate modeling is especially important. Modeling the complex dielectric permittivity and the loss tangent as frequency-independent values leads to non-causal results, which is especially problematic when accurate time-domain simulations are the goal [Hall], [Djordjević]. Therefore we focus on identifying a causal time-domain model. As a basis, we use the Kramers-Kronig relations [Ramo], which express a mathematical relationship between real and imaginary parts of the response functions. In this chapter, we use a recently published model for dielectric loss in printed circuit boards [Djordjević] to model the dielectric part of the cable loss. It is shown that the combination of the skin-effect model and this dielectric model gives a causal time-domain impulse response, using a minimum of model parameters.

Models only have meaning if they can accurately predict measurement results, so we need to thoroughly check the model predictions. We describe two types of measurements in this chapter: network analyzer measurements and time-domain Transmissometry (TDT) measurements. Each type of measurement has its particular use. A magnitude transfer plot gives direct insight into the channel loss at a certain frequency, for example at the Nyquist frequency. The time domain impulse response, on the other hand, gives a direct intuitive insight into intersymbol interference (ISI).

Concerning the frequency domain, measurement of the magnitude is more straightforward than of the phase. Due to the long propagation delay of the long cables that we use, and the high signal frequencies, the phase rotates very rapidly. Using this data to obtain the cable impulse response using an inverse Fourier transform can be hard, since the data needs to be corrected for noise and measurement artifacts. We can, of course, construct the 'minimum-phase' as described in [Bode] but without measuring we cannot be sure whether the cable is actually a minimum-phase network (after subtraction of the propagation delay). Therefore, we wish to avoid the need for accurate phase measurements. Our aim is to find a model which can be matched with only the measured magnitude, and then, after fitting the model, to obtain the phase from the model. This magnitude and phase information is then input to the inverse Fourier transformation.

Concerning the time domain, wideband (10GHz and higher) time-domain equipment has recently become available that enables direct measurement of the step response. Through differentiation, the impulse response can be obtained. The differentiation adds noise to the measurements, and the generated step has a limited rise time. This limits the accuracy of the time domain measurements so it is important to have frequency domain measurements as well. We fit the model with the measured frequency domain magnitude data and check it in the time domain against the measured impulse response. Measurements in both domains give more certainty in assessing the model's accuracy.

In this chapter, we model and measure coaxial cables, twisted pair cables, and printed circuit boards. It is shown that both the skin effect equations and the dielectric equations obey the Kramers-Kronig relations, guaranteeing causality.

In section 2.2 we first define the transfer function and the complex propagation constant in the RLGC form, and the constraints imposed on it by causality. Next, in section 2.3, all the RLGC parameters, and then the complete frequency domain transfer function (magnitude and phase) are calculated by analyzing both the skin effect and the dielectric loss. The subject of section 2.4 is the time domain impulse responses. Next, in section 2.5, measurement results are given for cables and printed circuit boards, and compared to the model.

2.2. Propagation constant and Kramers-Kronig relations

2.2.1. Propagation constant

The frequency domain transfer function *H(jω)* of a perfectly matched lossy copper transmission line is given by:

$$H(j\omega) = e^{-\gamma l}, \tag{1}$$

where l is the length of the cable, and *H(jω)* is defined as the ratio between the output and input voltages of the cable (V_{out} and V_{in} respectively):

$$H(j\omega) = \frac{V_{out}(j\omega)}{V_{in}(j\omega)}. \tag{2}$$

The complex propagation constant γ is defined as [Gardiol], [Grivet], [Chipman], [Ramo]:

$$\gamma = \sqrt{(R + j\omega L)(G + j\omega C)}, \tag{3}$$

where R is the distributed series resistance (Ω/m), L is the distributed inductance (H/m), G the distributed parallel conductance (S/m), and C the distributed capacitance (F/m), as shown in Fig. 1.

The actual values of the RLGC parameters are determined in the next sections, by analyzing the skin effect and the dielectric loss.

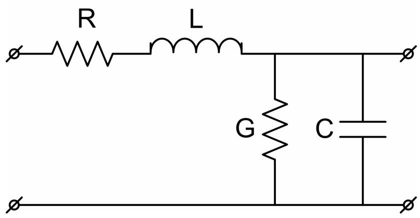

Fig. 1. RLGC representation of an infinitesimally small section of the transmission line.

2.2.2. Kramers-Kronig relations

The transfer function *H(ω)* is subject to a strict set of rules, because it is the Fourier transform of the transmission line's impulse response. This transmission line is a physical system, which imposes the two constraints described below.

(1) A physical system can only have a causal impulse response (no reaction before an action), so the following needs to be true:

$$h(t) = 0 \quad t < 0 . \tag{4}$$

This causality requirement for *h(t)* enforces a strict relation between the real and imaginary parts of its Fourier transform. This Fourier transform is a complex analytic function in the upper half plane.

(2) The impulse response of a physical system is a real function. As a result of this, its Fourier transform *H(ω)* has a special property. The values at positive frequencies are the complex conjugate of the values at negative frequencies:

$$H(-\omega) = H^{*}(\omega) . \tag{5}$$

When condition (1) is valid, the Kramers-Kronig relations apply to the real and imaginary parts of the Fourier transform [Ramo]. These mathematical relations connect the real and imaginary parts of a complex analytic function in the upper half plane for the response function [Arabi], [Djordjević]. They allow us to calculate the imaginary part of the response, knowing only the real part, and vice versa. They are a special case of the Hilbert transform [Djordjević]. The symmetry implied by condition (2) simplifies the Kramers-Kronig relations such that their integration interval runs from zero to plus infinity, instead of from minus infinity to plus infinity. For the complex function:

$$X(\omega) = X_r(\omega) + i \cdot X_i(\omega) , \tag{6}$$

the simplified Kramers-Kronig relations are [Ramo]:

$$X_r(\omega) = \frac{2}{\pi} PV \int_0^{\infty} \frac{\omega' X_i(\omega')}{\omega'^2 - \omega^2} d\omega' , \tag{7}$$

and

$$X_i(\omega) = -\frac{2}{\pi} PV \int_0^{\infty} \frac{\omega X_r(\omega')}{\omega'^2 - \omega^2} d\omega' , \tag{8}$$

where PV denotes the Cauchy principal value, necessary for calculation because the functions have a discontinuity at $\omega'=\omega$.

We use the Kramers-Kronig relations throughout the rest of this chapter, to make sure that we obtain a causal impulse response.

2.3. Frequency domain equations

In this section, we calculate the values for the RLGC parameters. First, in subsection 2.3.1, ‘R’ and ‘L’ is calculated by analyzing the skin effect, and next, in subsection 2.3.2, ‘C’ and ‘G’ is calculated by analyzing the dielectric loss.

2.3.1 Conductor losses: the skin effect

The skin effect is the phenomenon that the penetration depth of electromagnetic (EM) waves into a non-ideal conductor is dependent on the frequency, leading to a frequency dependent series resistance and inductance. High-frequency current flows only in the skin of the conductor; hence the term “skin effect”. It has effects on ‘R’ and on ‘L’: the decreasing EM wave penetration depth reduces the effective usable conductor area, while it also decreases the internal inductance (internal to the wire) and the magnetic field caused by this current. The skin effect was accurately described as long ago as 1934 [Schelkunoff]. For completeness, and for later use in our measurements, we give the formulas below.

In 2.3.1.1 we calculate the distributed resistance R and in 2.3.1.2 the distributed inductance L. Next, in 2.3.1.3, we show that the Kramers-Kronig relations hold for the complex impedance formed by R and L.

2.3.1.1. R: distributed resistance

In our analysis we first look at the effective conductor resistance. This resistance increases continuously with frequency. The current density decreases gradually from the skin to the conductor center. The effective wave penetration depth ∂_s, defined as the penetration distance at which the current density is attenuated by 1 neper (8.69dB), is related to angular frequency, electric conductivity σ and magnetic permeability μ as follows [Gardiol], [Grivet], [Chipman], [Ramo]:

$$\partial_s = \sqrt{\frac{2}{\omega \mu \sigma}} . \tag{9}$$

Combining penetration depth with wire radius, the skin effect cutoff angular frequency ω_{sa} (where the skin depth is equal to the radius) can be calculated for a circular conductor [Gardiol], [Grivet], [Chipman], [Ramo]:

$$\omega_{sa,x} = \frac{2}{x^2 \mu \sigma}, \tag{10}$$

where x is the radius of the conductor. The cutoff frequency is independent of cable length.

Well below this cutoff frequency, the EM waves use the whole conductor area and the distributed conductor resistance (without return path) is equal to its DC level [Gardiol], [Grivet], [Chipman], [Ramo]:

$$R_{DC,\sin gle} = \frac{1}{\sigma \pi x^2}. \tag{11}$$

For example, for the RG-58U coaxial cable, the cutoff frequency is as low as 22kHz. Above the cutoff frequency, the distributed AC wire resistance R_{AC} can be calculated as [Gardiol], [Grivet], [Chipman], [Ramo]:

$$R_{AC} = \lambda \sqrt{\omega}. \tag{12}$$

For a coaxial cable, λ is equal to [vdPlaats]:

$$\lambda_c = \frac{1}{2\pi}\left(\frac{1}{a} + \frac{1}{b}\right)\sqrt{\frac{\mu}{2\sigma}}, \tag{13}$$

where a is the radius of the center conductor, and b the distance from the center to the shield (see Fig. 2(a)). For the differential pair [vdPlaats]:

$$\lambda_d = \frac{2D}{\pi d \sqrt{D^2 - d^2}}\sqrt{\frac{\mu}{2\sigma}}, \tag{14}$$

where d is the diameter of the either one of the two conductors and D is the distance between the centers of the two conductors (see Fig. 2(b)).

For a PCB microstrip, the λ parameter is given by [Svensson]:

$$\lambda_p = \frac{1}{w}\sqrt{\frac{\mu}{2\sigma}}, \tag{15}$$

where w is the track width.

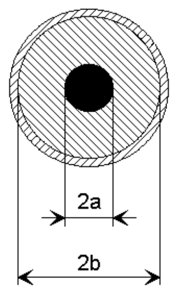

(a)

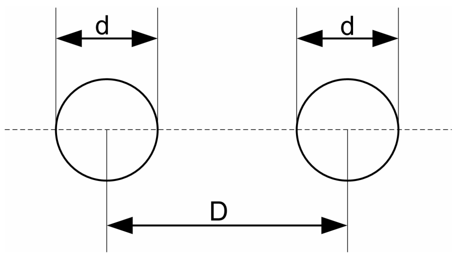

(b)

Fig. 2. Cable cross-sections. (a) Coaxial cable. (b) Differential pair.

2.3.1.2 L: distributed inductance

The total distributed conductor inductance L consists of an internal and external component [Gardiol], [Grivet], [Chipman], [Ramo]:

$$L = L_e + L_i \,. \tag{16}$$

The frequency-independent external inductance L_e characterizes the relation between external flux and total current in the conductor, and can be estimated for the coaxial cable as [Gardiol], [Grivet], [Chipman], [Ramo]:

$$L_{e,c} = \frac{\mu}{2\pi} \ln(b/a), \tag{17}$$

and for the differential pair [Gardiol], [Grivet], [Chipman], [Ramo]:

$$L_{e,d} = \frac{\mu}{\pi} \cosh^{-1}\left(\frac{D}{d}\right). \tag{18}$$

For estimating the distributed external inductance of the PCB microstrip, we can use the well known design rule [Johnson]:

$$L_{e,s} = 2 \cdot 10^{-7} \left(\frac{5.98d}{0.8w + h}\right), \tag{19}$$

where d is the trace height above the groundplane (dielectric distance) and h is the trace thickness.

The *internal* inductance L_i of the conductor is the relation between internal flux and current inside the conductor, and it is affected by the skin effect. This L_i is calculated as [Gardiol], [Grivet], [Chipman], [Ramo]:

$$L_i = \frac{\lambda}{\sqrt{\omega}} . \tag{20}$$

From Eq. 20, it can be seen that L_i decreases continuously with frequency.

2.3.1.3. Kramers-Kronig relations between R and Li

The Kramers-Kronig relations can be applied to the skin-effect formulas for R and L_i. For this purpose, we define the internal (skin) impedance Z_i as follows:

$$Z_i = R + j\omega L_i , \tag{21}$$

where R the resistance and L_i the internal inductance. Described in a different way, it is the ratio of the longitudinal potential difference over a unit length of the conductor to the longitudinal current in the conductor [Chipman]. To show that the internal impedance satisfies the Kramers-Kronig relations, we equate it with Eq. 6:

$$R + j\omega L_i = X_r(\omega) + jX_i(\omega) . \tag{22}$$

Substituting $X_r(\omega)=\lambda\sqrt{(\omega)}$ in Eq. 8, we obtain [vEtten]:

$$X_i(\omega) = -\frac{2}{\pi} PV \int_0^{\infty} \frac{\omega\lambda\sqrt{\omega'}}{\omega'^2 - \omega^2} d\omega' = \lambda\sqrt{\omega} , \tag{23}$$

which shows that the causality condition is satisfied, because:

$$j\omega L_i = j\omega\frac{\lambda}{\sqrt{\omega}} = \lambda\sqrt{\omega} = jX_i(\omega) . \tag{24}$$

(Compare Eq. 20.)

Alternatively, the relation can be considered from the viewpoint of the conservation of energy [Ramo]. The internal (skin) impedance has to obey the law of the conservation of energy. The energy that is dissipated by the resistance cannot be stored in the magnetic field [Hall]. Thus when the resistance increases with increasing frequency, the internal inductance needs to decrease.

With a real conductance σ, the resistance and internal reactance of a plane conductor are equal at any frequency [Ramo]. Therefore the internal impedance always has a phase angle of 45 degrees.

2.3.2. Dielectric Loss

Continuing the calculation of the RLGC parameters, we now calculate the 'C' and 'G' parameters by analyzing the second loss effect: the dielectric loss.

The dielectric loss is caused by the conversion of electrical energy to other domains by the dielectric between the two conductors in the cable, mainly as a consequence of dielectric polarization and relaxation.

A crossing frequency can be found beyond which the dielectric loss starts to predominate over the skin effect. The skin effect dominates at low frequencies in any cable, and dielectric loss dominates at high frequencies. Therefore, for cables errors in modeling the dielectric loss are usually not very visible. For high speed serial links over printed circuit board traces, the situation is different. The dielectric in FR4, made from glass fiber and epoxy, has much higher loss than the polyethylene or specially designed low-loss (foamed or air) dielectric in cables. Therefore, in FR4, the dielectric loss predominates over the skin loss already at low frequencies. The recent work on high-speed broadband cable and backplane data-communication systems has revitalized interest in channel models that remain accurate in the GHz range. Indeed, it is a very topical subject: recently many publications have been devoted to the challenge of modeling dielectrics [Djordjević], [Hall]. Jonscher wrote in 1999 that 'dielectric relaxation in solids represents one of the most intensely researched topics in physics' [Jonscher].

In 2.3.2.1, the distributed capacitance C is calculated. In 2.3.2.2, the distributed shunt conductance G is calculated, and the modeling of the loss tangent is discussed.

2.3.2.1. C: the distributed capacitance

For calculating the distributed capacitance C, we first introduce the frequency-dependent complex dielectric permittivity ε, which is dependent on the dielectric material:

$$\varepsilon(\omega) = \varepsilon' - j\varepsilon''. \tag{25}$$

The distributed parallel capacitance in a coaxial cable is given by [Gardiol], [Grivet], [Chipman], [Ramo]:

$$C_c(\omega) = \frac{2\pi\varepsilon'}{\ln(b/a)}, \tag{26}$$

and, for a differential pair, by [Gardiol], [Grivet], [Chipman], [Ramo]

$$C_d(\omega) = \frac{\pi\varepsilon'}{\cosh^{-1}\left(\frac{D}{d}\right)}. \tag{27}$$

For the estimating the distributed capacitance of the PCB microstrip, we can use the well known design rule [Johnson]:

$$C_s(\omega) = \frac{2.64\cdot 10^{-11}\left(\frac{\varepsilon'}{\varepsilon_0}+1.41\right)}{\ln\left(\frac{5.98d}{0.8w+h}\right)}. \tag{28}$$

2.3.2.2. G: distributed shunt conductance

The last remaining RLGC parameter is G, the distributed shunt conductance. It is calculated using the frequency-dependent loss tangent. The definition of the loss tangent is:

$$\delta(\omega) = \frac{\varepsilon''}{\varepsilon'} . \tag{29}$$

The frequency-dependent shunt conductance per meter G is given by [Gardiol], [Grivet], [Chipman], [Ramo]:

$$G(\omega) = \delta\omega C . \tag{30}$$

In some older publications [Brianti], [vdPlaats], the loss tangent is incorrectly assumed to be a constant and as a result, the dielectric part of the transfer function is modeled as linearly dependent on frequency and considered to be non-dispersive. An inverse Fourier transform then (incorrectly) yields a symmetrical impulse response. A dielectric attenuation linearly dependent on ω is physically impossible. The Paley-Wiener criterion and Kramers-Kronig relations dictate that no causal network can provide an attenuation which (asymptotically) increases as a function of ω with a factor larger than or equal to one times ω [Guillemin], [Nahman].

To guarantee causality in the time domain, the real and imaginary parts of the complex dielectric permittivity function again need to form a Kramers-Kronig pair [Ramo]. This can also be understood from another point of view. The conservation of energy law also dictates a necessary relation between *ε'* and *ε"*. The energy that is dissipated in the dielectric cannot be stored on its capacitance. When the real part of the dielectric permittivity decreases, less energy can be stored capacitively and the dielectric losses increase, indicated by an increase in the imaginary part of the dielectric constant [Hall].

To obtain a dielectric response that does comply with Kramers-Kronig, the response can be modeled as a sum of multiple single Debye responses, each with a different relaxation time [Svensson], or a continuous sum of an infinite number of Debye responses [Djordjević]. Although [Jonscher] notes that this distributed relaxation times approach "fails to address the evident existence of a universal fractional power-law behavior which represents very well the high-frequency dipolar behavior", at present it does seem to be the most practical approach. In their papers, [Svensson] and [Djordjević] show their model to correspond well with measurements.

The complex, frequency-dependent dielectric permittivity of FR4 is approximated as follows [Djordjević], as published in 2001:

$$\varepsilon(\omega) = \varepsilon' - j\varepsilon'' = \varepsilon'_{\infty} + \frac{\Delta\varepsilon'}{m_2 - m_1}\log_{10}\left(\frac{\omega_2 + j\omega}{\omega_1 + j\omega}\right), \tag{31}$$

where $\Delta\varepsilon'$ is the total variation of ε between the lower ($\omega_1 = 10^{m1}$) and upper model frequency ($\omega_2 = 10^{m2}$), and ε'_{∞} is the dielectric constant at very high frequencies. This equation for ε obeys the Kramers-Kronig relations.

Although the above function is meant for modeling the complex dielectric permittivity in FR4, it was also found to be useful and accurate to model the dielectric in cables. We use Eq. 31 to calculate the frequency-dependent values for C and G. The optimum values for the parameters in Eq. 31 are determined experimentally, to fit with the measurements.

2.3.3. Isolated magnitude transfer function for skin loss and dielectric loss

It is important to be able to see in the frequency domain magnitude plot the separate contributions of skin-effect and dielectric-loss. We could, for example, determine which loss mechanism is dominant and at which 'crossing frequency' the dielectric loss starts to dominate over the skin-effect loss.

Having found all the RLCG parameters, we can collect them together and substitute them into Eq. 3 for the propagation constant, which leads to:

$$\gamma = \sqrt{\left(\lambda\sqrt{\omega} + j\omega\left(L_e + \frac{\lambda}{\sqrt{\omega}}\right)\right)\left(\delta\omega C + j\omega C\right)}, \tag{32}$$

where C is frequency-dependent through ε (using Eq. 31), and δ is also frequency-dependent. (See Eq. 29.) The above formula can be rewritten as

$$\gamma = j\omega\sqrt{L_e C\left(1 + \frac{(1-j)\lambda}{L_e\sqrt{\omega}}\right)\left(1 - j\delta\right)}. \tag{33}$$

The loss contributions in the propagation constant can be separated by using a binomial series approximation. Using the binomial series for power 0.5, valid for small x:

$$\sqrt{1+x} = 1 + \frac{x}{2} - \frac{1}{8}x^2 + \frac{1}{16}x^3 + \ldots, \tag{34}$$

we obtain [vdPlaats]

$$\gamma = j\omega\sqrt{L_e C}\left(1 + \frac{(1-j)\lambda}{2L_e\sqrt{\omega}} - \frac{(1-j)^2\lambda^2}{8L_e^2\omega} + \ldots\right)\left(1 - j\frac{\delta}{2} + \frac{\delta^2}{8} + \ldots\right). \tag{35}$$

The series can be truncated after the $x/2$ term, because the further terms are negligible, resulting in [vdPlaats]:

$$\gamma = \underbrace{j\omega\sqrt{L_e C} + j\frac{\lambda}{2}\sqrt{\frac{C}{L_e}}\sqrt{\omega}}_{j\beta} + \underbrace{\frac{\lambda}{2}\sqrt{\frac{C}{L_e}}\sqrt{\omega} + \frac{\delta\omega}{2}\sqrt{L_e C}}_{\alpha}, \tag{36}$$

where the accolades indicate the loss terms α and the phase terms β.

(As an aside - because C is a (weak) function of ω, because it is calculated using Eq. 31, as stated above, we cannot simply state that the propagation delay is given by the first phase term in the above equation. In fact, that term also captures the dispersion from the dielectric loss. This is not a problem here because we are only interested in the magnitude.)

We take the loss terms (the third and forth terms) because we are interested in the magnitude transfer function. The frequency domain magnitude transfer function is now written as:

$$\left|H(\omega)\right| = e^{\left(\frac{\lambda}{2}\sqrt{\frac{C}{L_e}}\sqrt{\omega}+\frac{\delta\omega}{2}\sqrt{L_e C}\right)l} . \tag{37}$$

In this equation, we can see the separate contributions for the skin-effect loss and the dielectric loss. To see only the dielectric loss, we set the conductivity σ to infinity, so that λ=0. The dielectric loss contribution is then:

$$\left|H_{diel}(\omega)\right| = e^{\left(\frac{\delta\omega}{2}\sqrt{L_e C}\right)l} . \tag{38}$$

To see only the skin-effect loss, we set the loss tangent δ to zero, resulting in:

$$\left|H_{skin}(\omega)\right| = e^{\left(\frac{\lambda}{2}\sqrt{\frac{C}{L_e}}\sqrt{\omega}\right)l} . \tag{39}$$

2.4. Time domain equations

The impulse response can be obtained from the transfer function from Eq. 1 above by a (numerical) inverse Fourier transform. We use this in the measurement section. However, for quick time-domain simulations, it can also be useful to have an analytical formula for the impulse response. In this section, we deal with the impulse responses for the skin effect (subsection 2.4.1) and for the dielectric loss (subsection 2.4.2).

2.4.1. Skin-effect impulse response

Well known from the literature is the skin-effect step response *a(t)* [Gardiol], [Grivet], [Chipman], [Ramo]:

$$a(t) = erfc(\sqrt{\tau_1 / t} / 2) . \tag{40}$$

This function is illustrated in Fig. 3(a). By differentiating this equation we obtain the (causal) skin-effect impulse response $h_1(t)$ [vdPlaats]:

$$h_1(t) = \frac{\sqrt{\tau_1}}{2t\sqrt{\pi t}} \cdot e^{-\frac{\tau_1}{4t}} , \tag{41}$$

where the skin-effect time constant τ_1 is equal to:

$$\tau_1 = \frac{l^2 \lambda^2}{2 Z_c^2} , \tag{42}$$

where $Z_c = \sqrt{L_e / C}$ approximates, at high frequencies, the characteristic impedance.

Fig. 3(b) shows $h_1(t)$. The x-axis shows time divided by τ_1. The y-axis shows $h_1(t)\cdot\tau_1$. The axis is chosen in this way to clearly show the maxima and time span of the function. It can be seen that $h_1(t)$ is asymmetrical over time with a very long tail.

In fact, 'time constant' τ_1 is not constant but is dependent on frequency through the frequency-dependent electrical capacity C. We test the accuracy of this simplification later in this chapter, but for now we state that for channels that are dominated by skin-effect loss, such as high-quality cables, $h_1(t)$ as given above is an accurate approximation of the impulse response.

In Chapter 4 we use this analytical skin-effect impulse response in time-domain simulations to analyze the PWM equalizer.

As an interesting aside, in Appendix A it is shown that a characteristically terminated on-chip RC line has exactly the same response as a skin-effect-only channel. Both channels can be described by means of a diffusion equation.

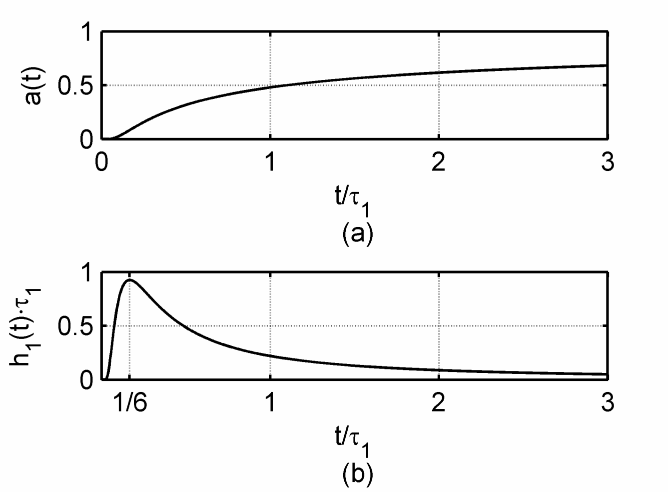

Fig. 3. Skin effect step response and impulse response. (a) Step response. (b) Impulse response.

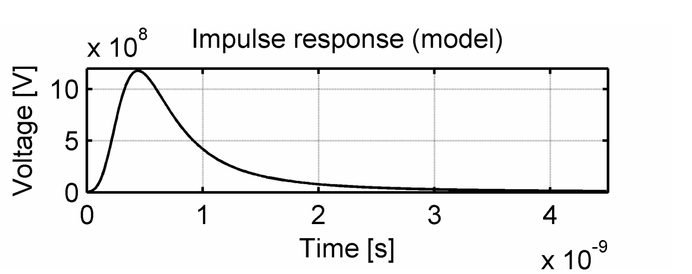

Fig. 4. Example of the theoretical, isolated impulse for dielectric loss.

2.4.2. Impulse response for dielectric loss

Unlike the skin-effect impulse response, the analytic impulse response of a channel dominated by dielectric loss could not be found in the literature. For an intuitive insight into the behavior of these channels, it would be convenient to know which shape this impulse response has. To obtain the impulse response, we first set the skin loss to zero by setting the conductivity to infinity, which results in R=0 and L_i=0. The propagation constant then becomes:

$$\gamma_{diel} = \sqrt{(j\omega L_e)(G + j\omega C)}\,, \tag{43}$$

and the accompanying dielectric-only transfer function is:

$$H_{diel}(j\omega) = e^{-\gamma_{diel} l}\,. \tag{44}$$

Taking the inverse Fourier transform of this equation yields the isolated dielectric impulse response. Like the skin-effect impulse response, it is also asymmetrical over time, with a long tail on the right side. The rise time is a bit longer and the function is less steep on the left side. See Fig. 4 for an illustration of an example. (In that figure, the propagation delay is subtracted from the time.)

2.5. Match between model and measurements

In this section, we compare the model with measurements of copper channels. Both time domain and frequency domain measurements are used. Measurements are made on four cables and a printed circuit board trace. First, in subsection 2.5.1, the measured channels are described. Next, in subsection 2.5.2, the measured transient responses to a random sequence of bits are given. Finally, in subsection 2.5.3, the measurements of the transfer functions S_{21} and the step responses are discussed and we check how well the model results match the measurements.

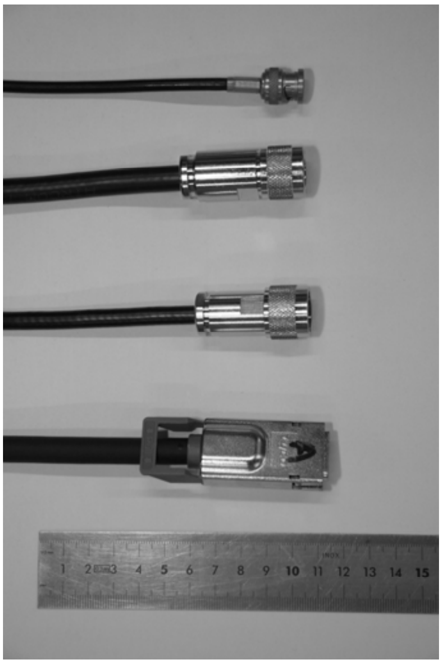

Fig. 5. From top to bottom: RG-58CU, Aircom+, Aircell7, 10GBASE-CX4.

2.5.1. Copper channel types

We measure four copper cables and one printed circuit board. We use two types of copper cables in our measurements: coaxial and differential cables. A photo of the cables and connectors is shown in Fig. 5, and the PCB trace is shown in Fig. 6. The five channels are:
(a) 25m RG-58CU (coaxial cable)
(b) 130m Aircom+ (coaxial cable)
(c) 80m Aircell7 (coaxial cable)
(d) 15m 10GBASE-CX4 (24AWG shielded differential cable)
(e) 270cm 50Ω FR4 PCB microstrip.

Table 1 shows the channel parameters and the parameters of the model fit, described later in the measurement section of this chapter. Cable (a) is a low-cost, low-end, standard coaxial cable with polyethylene dielectric. Cable (b) is a more expensive coaxial cable with low-loss air dielectric, designed for frequencies up to 10GHz. However, it is rather rigid and has a large diameter. Cable (c) has a foam dielectric and an inner conductor of woven copper. Therefore it is much more flexible and thinner than (b), while still offering a low dielectric loss relative to cable (a). Finally cable (d) contains 8 shielded differential pairs and is designed for a bit rate of 3.125 Gb/s per pair using 2-tap SSF at the transmitter. A small adapter PCB makes one of the pairs available at an SMA connector. All coaxial cables and the PCB trace have a characteristic impedance of 50Ω and (d) has a differential characteristic impedance of 100Ω. Cable (d) was not available at lengths of more than 15m. Channel (e) is a printed circuit board with the widely used FR4 type dielectric. We used a very long pcb trace of 270cm (106”) to be able to achieve a high channel loss at the Nyquist frequency. The trace is single-ended. It is a microstrip with a characteristic impedance of 50Ω. There are no vias, and at both ends there are SMA connectors.

Reflections were reduced to a minimum by choosing channels with well controlled characteristic impedances and terminating them with well matched resistors.

Chapter 4 describes how these channels are used to determine the performance of the equalizer. For this purpose, we needed to use a number of channels that are different in terms of physical configuration and skin effect / dielectric loss ratios. The lengths of the coaxial cables are chosen such that the equalizer can be tested at the highest speed and maximum loss compensation that it can handle. The PWM equalizer can typically handle up to 30dB of loss at 5Gb/s, as is shown later.

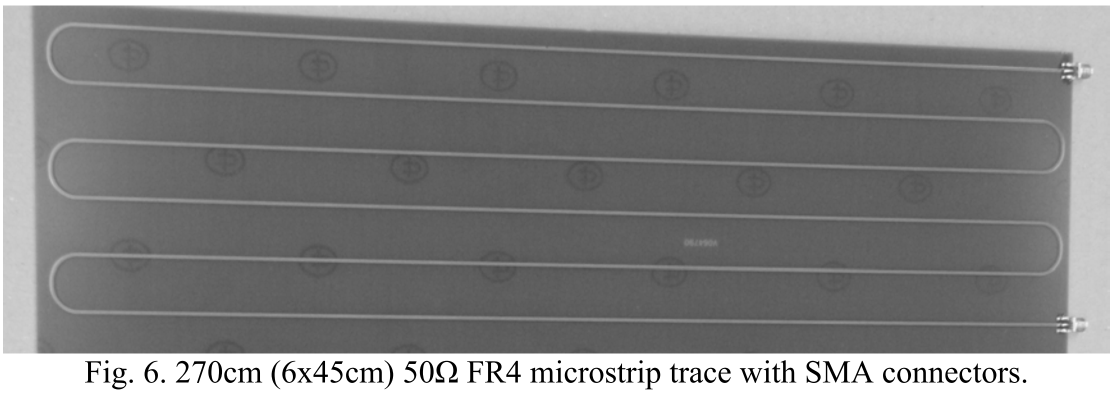

Fig. 6. 270cm (6x45cm) 50Ω FR4 microstrip trace with SMA connectors.

Name	(a)	(b)	(c)	(d)	(e)
Type	**RG-58CU**	**Aircom+**	**Aircell7**	**10GBASE-CX4**	**PCB microstrip**
Physical parameters					
Length	25m	130m	80m	15m	270cm
Conduct. (σ)	$5.8\ 10^7$	$5.8\ 10^7$	$5.8\ 10^7$	$5.8\ 10^7$	$5.8\ 10^7$
Cable outer diameter	5.1mm	10.3mm	7.3mm	10mm (8 pairs)	n/a
Radius inner conductor *(a)*	0.45mm (woven)	1.35mm (solid)	0.93mm (woven)	n/a	n/a
Radius outer conductor *(b)*	1.48mm	3.6mm	2.5mm	n/a	n/a
Diameter of cond. (d)	n/a	n/a	n/a	0.51mm (24AWG)	n/a
Dist. between cond. (D)	n/a	n/a	n/a	0.8mm	n/a
Width (w)	n/a	n/a	n/a	n/a	1.2mm
Dielectric distance (d)	n/a	n/a	n/a	n/a	0.8mm
Thickness (h)	n/a	n/a	n/a	n/a	45um
Dielectric	Polyethylene	Air	Foam	Foam	FR4
Measured parameters					
Loss/10m @2.5GHz	12.4dB	2.3dB	3.7dB	12.7dB	74.1dB
Calculated from physical parameters					
λ	$4.80\ 10^{-5}$	$1.69\ 10^{-5}$	$2.45\ 10^{-5}$	$1.69\ 10^{-4}$	$8.74\ 10^{-5}$
L_e	$2.37\ 10^{-7}$	$1.96\ 10^{-7}$	$1.99\ 10^{-7}$	$4.09\ 10^{-7}$	$3.13\ 10^{-7}$
Model fit parameters					
$\varepsilon_r'_\infty$	2.6	1.4	1.5	2.1	4.0
$\Delta\varepsilon_r'$	$81\ 10^{-3}$	$4.5\ 10^{-3}$	$7.9\ 10^{-3}$	$21\ 10^{-3}$	1.5
m_1	1.7	1.5	3.8	3.3	1.1
m_2	14	14	14	14	14
τ_1	1.0ns	1.3ns	1.2ns	0.63ns	0.5ns

Table 1. Channel parameters.

2.5.2. Transient behavior

To obtain a first impression of their transient behavior, the measured response of the four cables and the PCB to a 2PAM random sequence of bits is given. See Figs. 7-11 below.

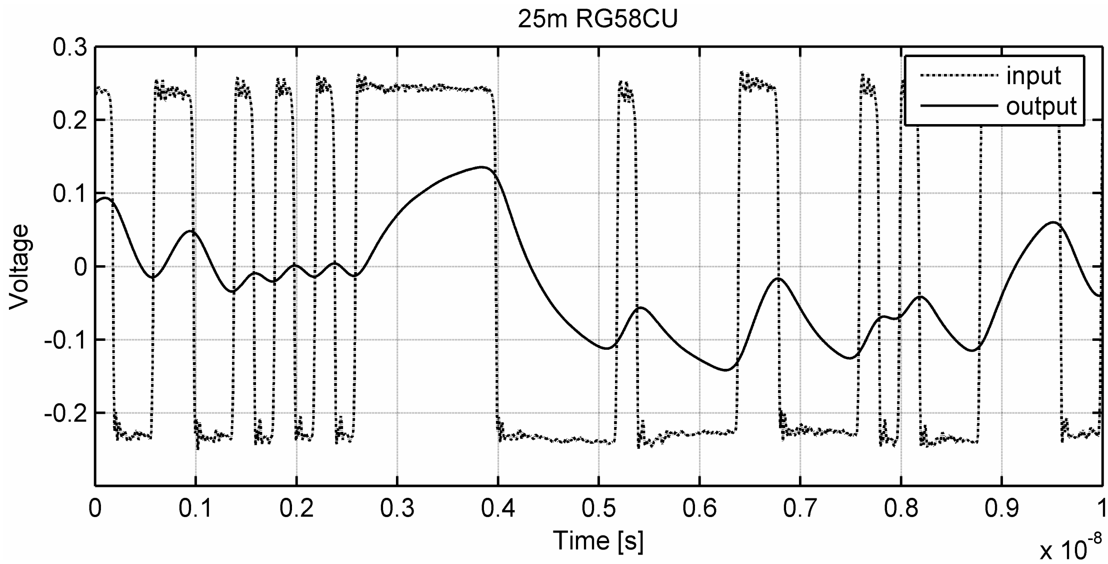

Fig. 7. Measured response of 25m RG58CU coaxial cable (a).

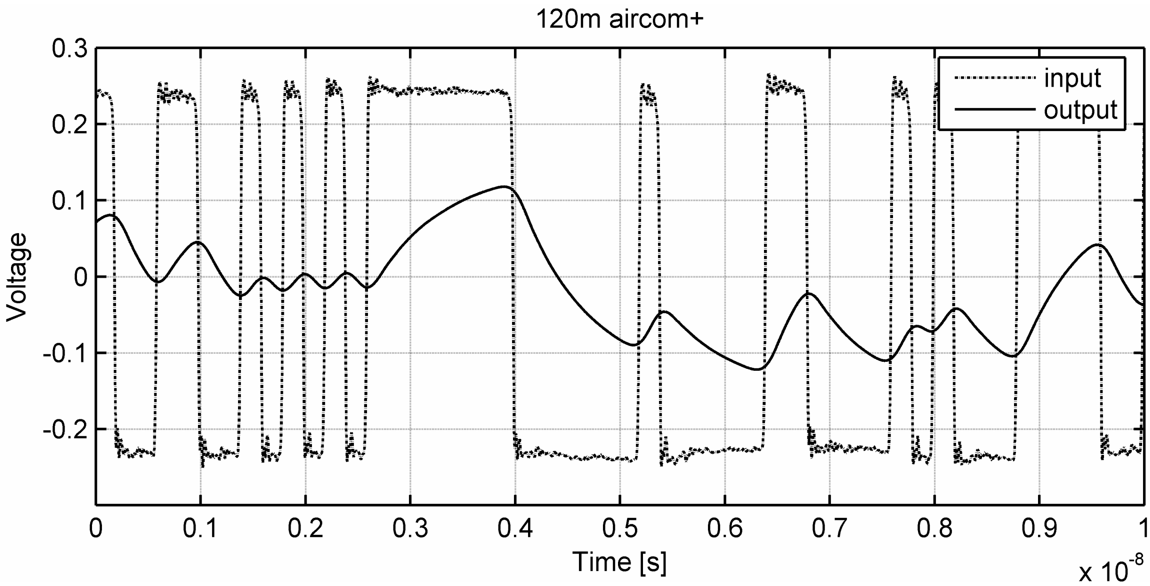

Fig. 8. Measured response of 120m Aircom+ coaxial cable (b).

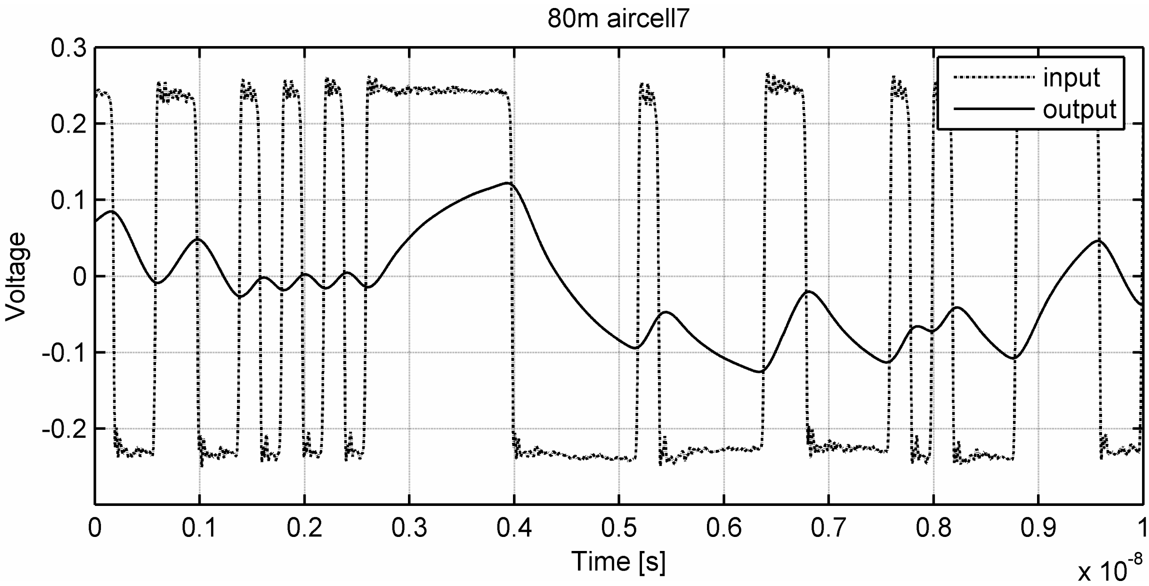

Fig. 9. Measured response of 80m Aircell7 coaxial cable (c).

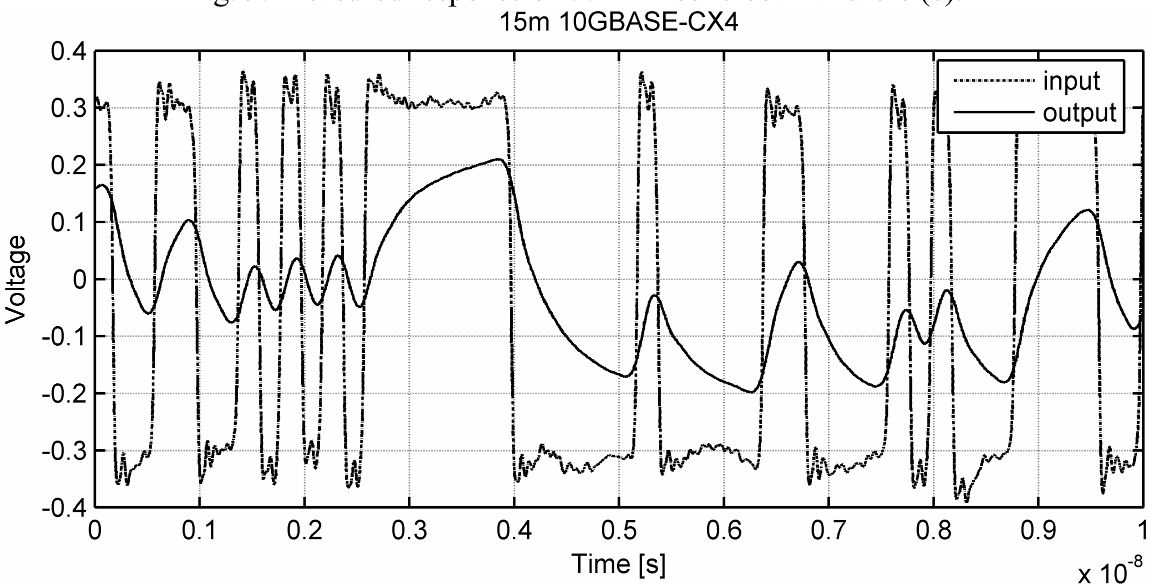

Fig. 10. Measured response of 15m 10GBASE-CX4 differential cable (d).

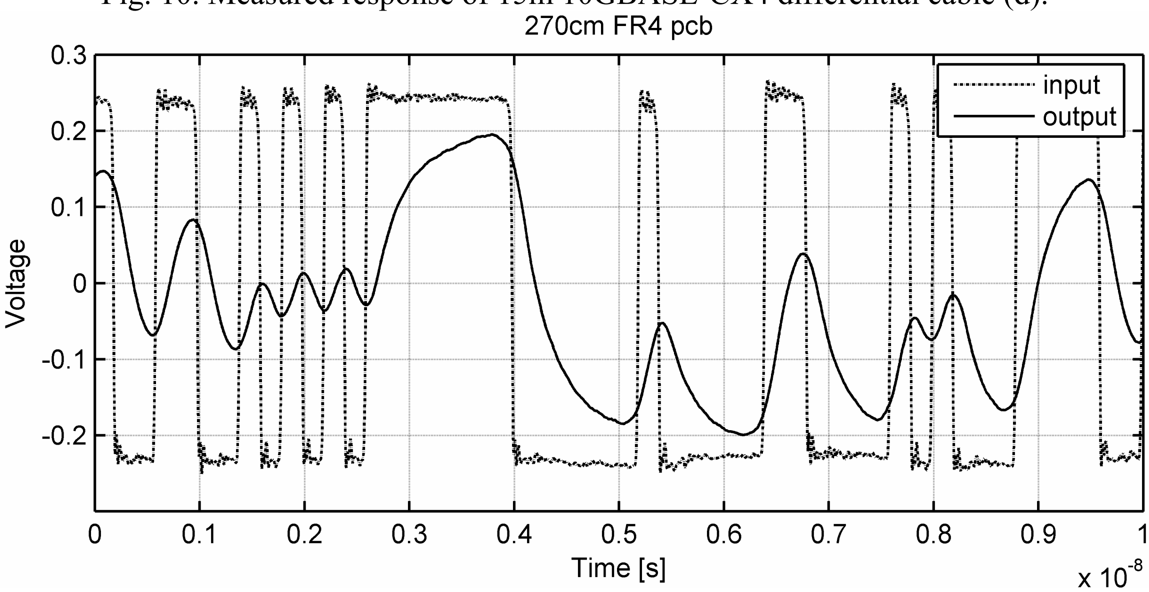

Fig. 11. Measured response of 270cm FR4 pcb trace (e).

In all cases, heavy ISI can be seen in the measurements. The amplitude of the output is higher for the twisted pair and the PCB channels, because of their lower losses, as is confirmed later by the S_{21} measurements. Furthermore, a slightly higher ripple can be seen in the PCB measurements. This is due to the better shielding of the cables.

2.5.3. Measurements – model match

A comparison is made between the measurements and the model using the three-step methodology described below.

(1) A measurement of the S_{21} (magnitude of the transfer function) of the channel is made using a network analyzer. The magnitude of the theoretical RLGC transfer function is fitted to it by adjusting the model parameters. Measurements and model fit are plotted in a figure. Using the equations from subsection 2.3.3, the skin loss and dielectric loss are calculated separately and also plotted.

(2) The step response of the cables is measured using time domain transmissometry (TDT). The impulse response is obtained by differentiation and (low-pass) noise filtering. This impulse response is compared with two theoretical impulse responses. The first is the inverse Fourier transform of the RLGC transfer function, used in step (1) above, calculated numerically. The second is the simple analytical skin effect impulse response given in subsection 2.4.1.

(3) Finally, the measured impulse response is Fourier transformed to obtain the frequency domain magnitude transfer. This is again compared to the frequency domain measurements in step (1).

2.5.3.1. S_{21} fit

In Figs. 12-16, the measured and modeled magnitudes of the transfer function S_{21} for the cables are shown, as described in step (1). The modeled contribution of conductor losses and dielectric losses is shown separately, using the equations from subsection 2.3.3. The measured and Fourier transformed impulse responses, as described in step (3), are also shown in this figure.

The legend for Figs. 12-16 is as follows:

- ‘model’: magnitude of Eq. 1,
- ‘model (skin)’: Eq. 39,
- ‘model (diel)’: Eq. 38,
- ‘measured (NA)’: measured using network analyzer,
- ‘measured (FT ht)’: measured using TDT and then Fourier transformed (see also subsection 2.5.3.2).

See Table 1 for the parameters that were used to fit the model. The optimization algorithm that was used for the model parameter fitting is Particle Swarm Optimization (PSO) [Kennedy]. The model parameters $\varepsilon_r'_\infty$, $\Delta\varepsilon_r'$ and m_1 for the dielectric loss were optimized to provide a model fit, while m_2 was fixed at 14 and the skin loss was fixed using the well known copper conductivity σ=5.8 10^7 S/m. When parameter $\varepsilon_r'_\infty$ is averaged over the whole frequency range, it comes very close to the commonly known values for the relative dielectric permittivity ε_r. These values are 2.25 for polyethylene in RG58CU, 1.4 for foam/air dielectric in Aircell7 and Aircom+, and 4.9 for FR4.

The dielectric loss of the PCB trace is lower than expected. It was designed for 30dB loss at 2.5GHz, using a loss tangent of 0.025. The measured loss is 21dB instead, so the dielectric loss is lower in this specific board. (In Chapter 4 the total channel loss is 25dB because a 1.75m coaxial cable and a bias tee are also used for connecting to the chip.)

Figs. 12-16 show the measurements and model fits in the frequency domain for 25m RG-58CU, 80m Aircell7, 130m Aircom+, 15m 10GBASE-CX4, and 270cm FR4 microstrip trace respectively. The measured network analyzer data and the modeled transfer function only differ significantly for RG-58CU above 2.5GHz. It is most likely that its BNC connectors cause impedance mismatches at those frequencies.

The Fourier transformed time domain measurements – from step (3), shown in the figures as 'FT ht' – differ slightly from the network analyzer data. A possible cause for this is that this result is calculated using the response to a non-ideal step, with finite steepness. For the PCB and the twisted pair (10GBASE-CX4), the difference is somewhat larger. It is most probably caused by the short pieces of coaxial cable needed to connect them to the TDT equipment. From the frequency domain measurements with the network analyzer, the effect of these short cables was removed by calibration, but from the TDT measurements it was not. However, in all cases the difference is not greater than 1-2 dB at 2.5GHz.

Cable (b) has the highest ratio of skin loss to dielectric loss, because of its air dielectric. Cable (a) has the crossing point between skin loss and dielectric loss at the lowest frequency of the copper cables, at 2.2GHz. Losses from the printed circuit board trace (e) are clearly dominated by dielectric losses.

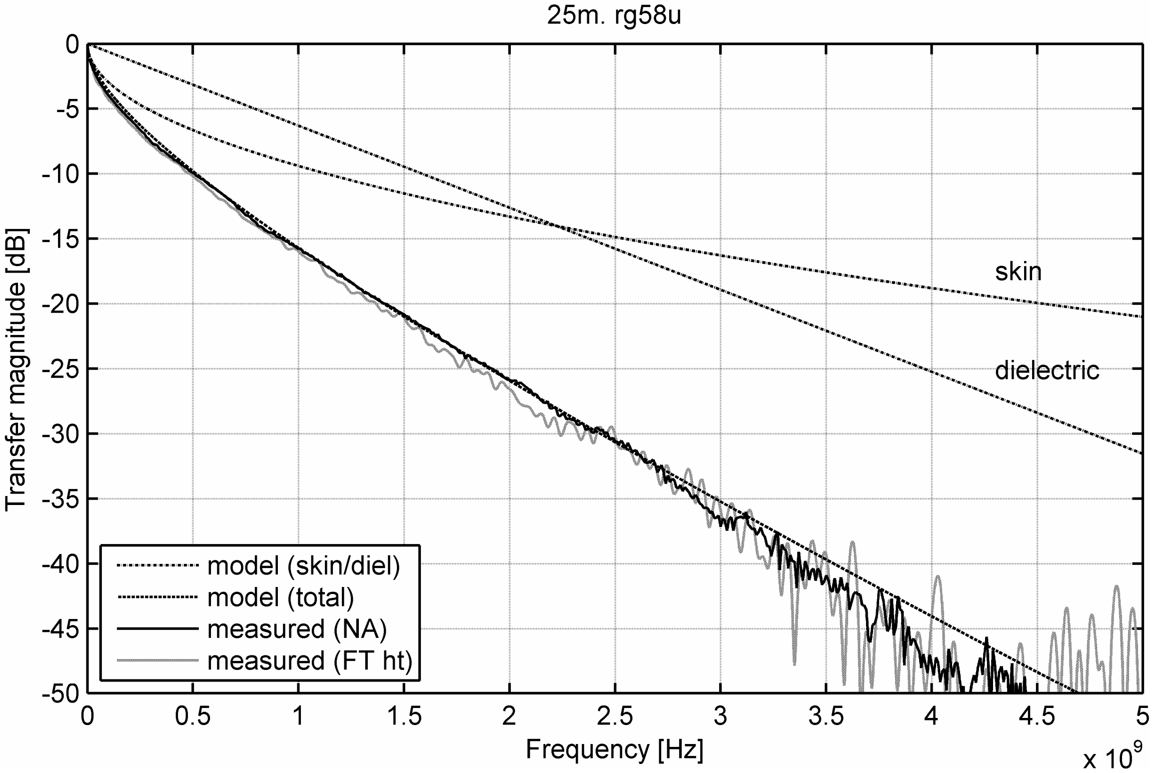

Fig. 12. Measured S_{21}, Fourier transform of measured impulse response, and model fit for 25m RG-58CU cable (a).

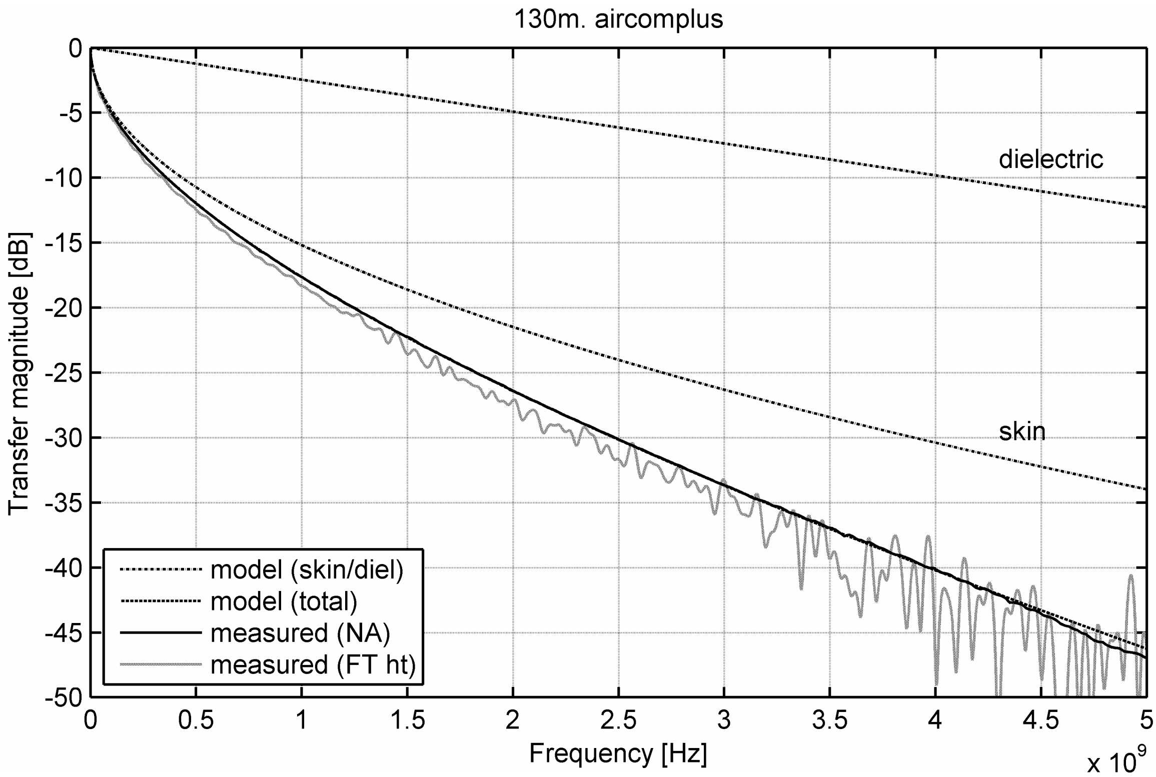

Fig. 13. Measured S_{21}, Fourier transform of measured impulse response, and model fit for 130m Aircom+ cable (b).

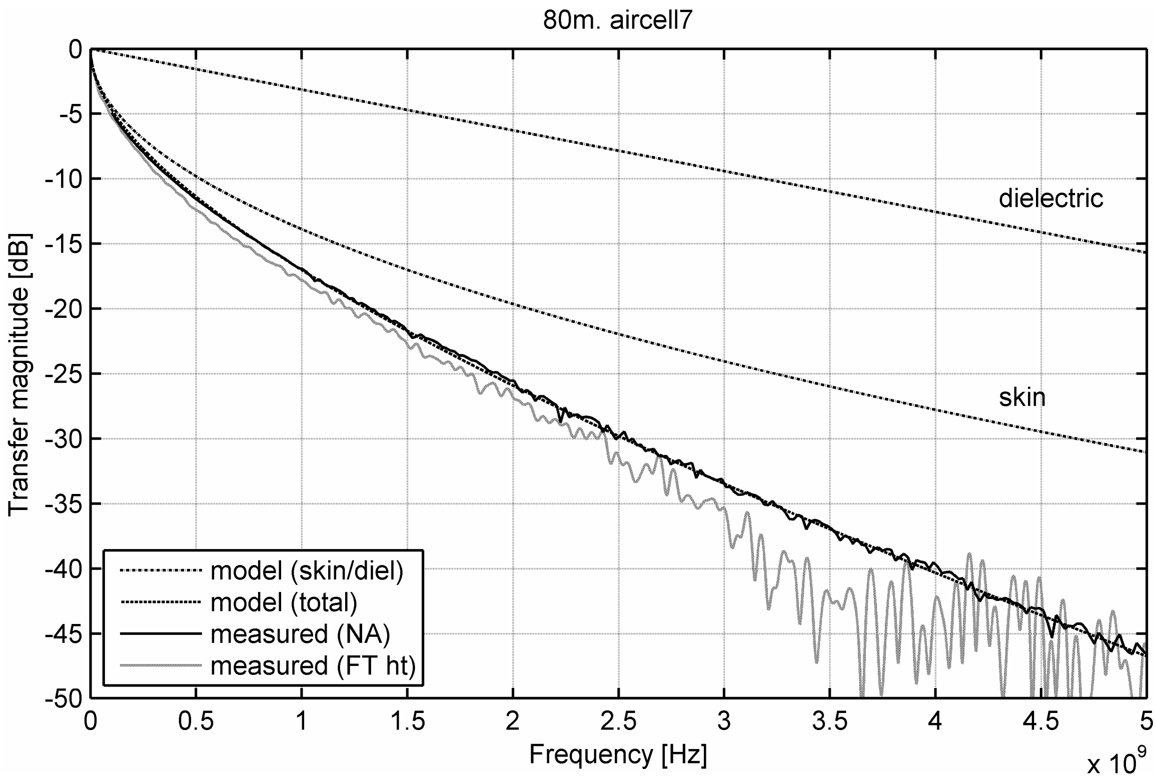

Fig. 14. Measured S_{21}, Fourier transform of measured impulse response, and model fit for 80m Aircell7 cable (c).

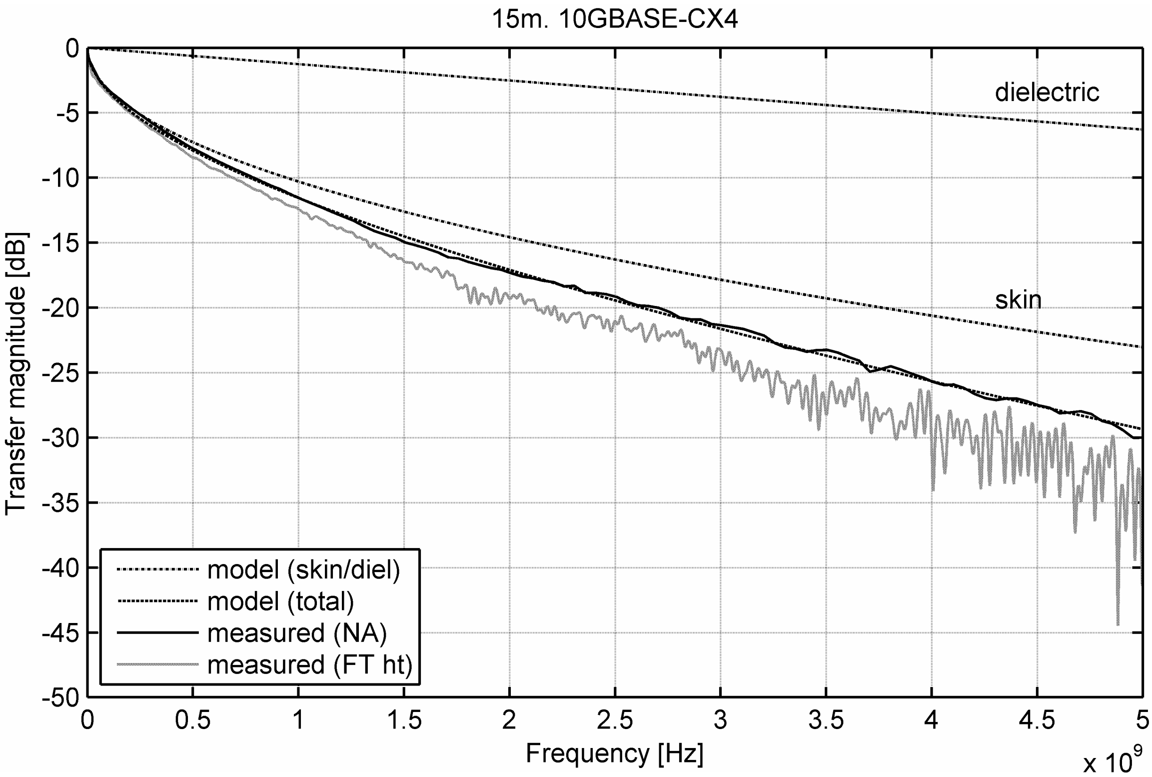

Fig. 15. Measured S_{21}, Fourier transform of measured impulse response, and model fit for 15m 10GBASE-CX4 24AWG (d). (Measured: S_{dd21}.)

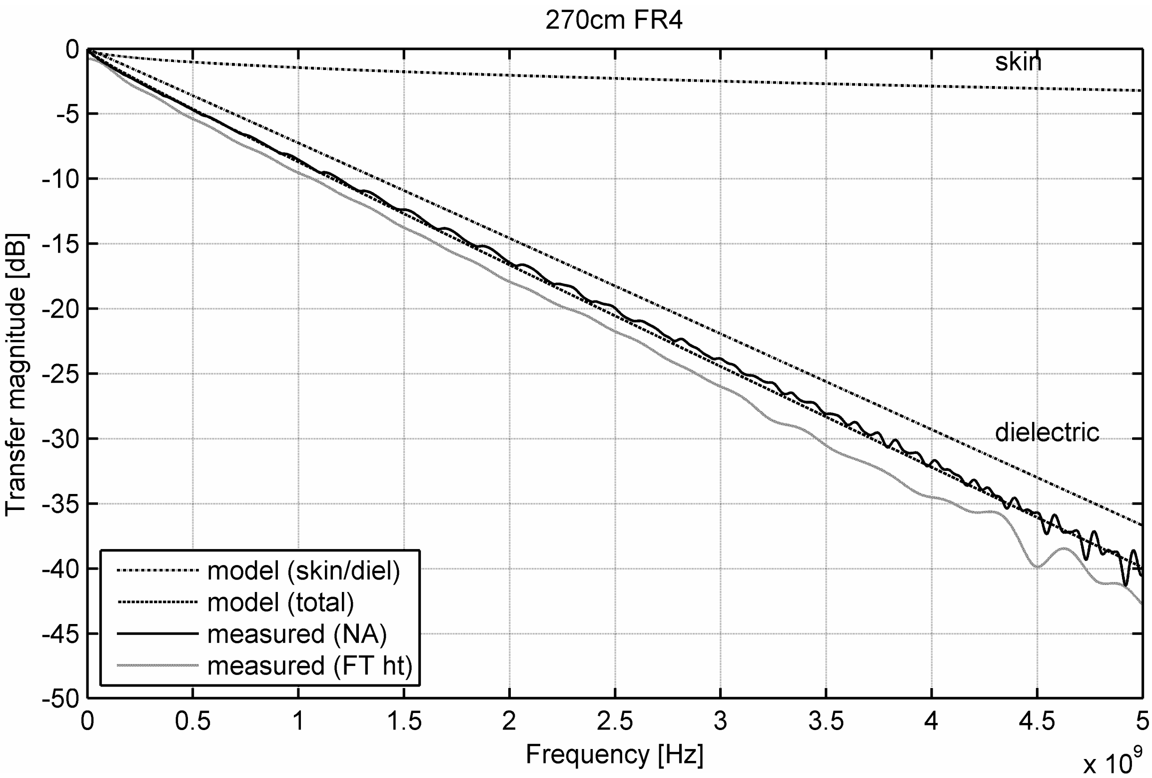

Fig. 16. Measured S_{21}, Fourier transform of measured impulse response, and model fit for 270cm long microstrip on FR4 printed circuit board (e).

2.5.3.2. Impulse response fit

For step (2) we show the time domain measurements and compare them to the models. A 40ps-risetime, 200ps step was used to measure the step responses. The measured step response was then differentiated to obtain the impulse response. To remove the high-frequency noise on this impulse response, a linear-phase equiripple low-pass FIR filter was used with a passband of 10GHz (0.01dB ripple), and 20dB attenuation in the stopband (starting at 15GHz). Figs. 17-21 show the results.

The legend for Figs. 17-21 is as follows:

- 'measured': impulse response from differentiated, noise filtered, step response,
- 'model (total)': numerically calculated inverse Fourier transform of Eq. 1 (of which the magnitude was fitted to the measured S_{21} in step (1); includes both skin effect and dielectric loss.
- 'model (skin)': Theoretical impulse response for isolated skin effect (subsection 2.4.1), calculated using parameter τ_1 in Table 1.

While most of the modeled impulse responses fit well with those from measurements, there is a small difference for both the 10GBASE-CX4 cable and the FR4 trace. As explained in the previous subsection, a likely cause is that they needed to be connected to the measurement equipment using short coaxial wires (20cm long). The effect of these short cables was removed by calibration from the network analyzer measurements, but not from the step response measurements.

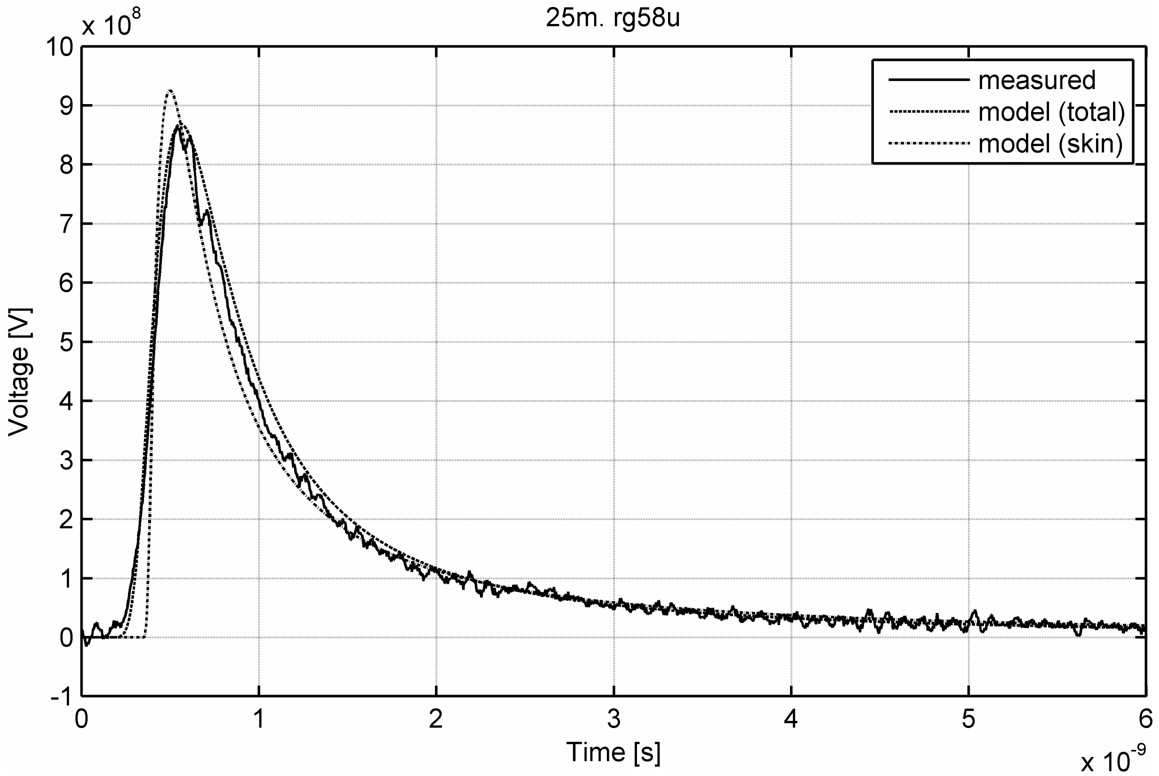

Fig. 17. Impulse response from measurements and model fit for 25m RG-58CU cable (a).

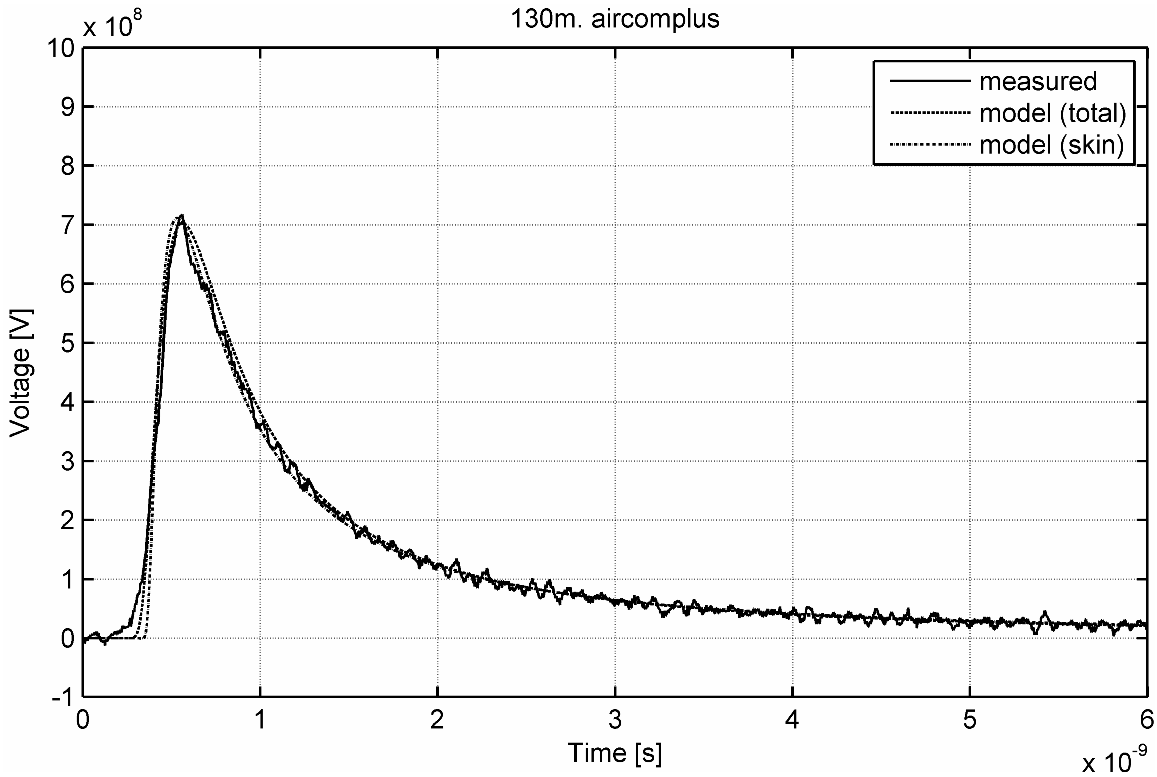

Fig. 18. Impulse response from measurements and model fit for 130m Aircom+ cable (b).

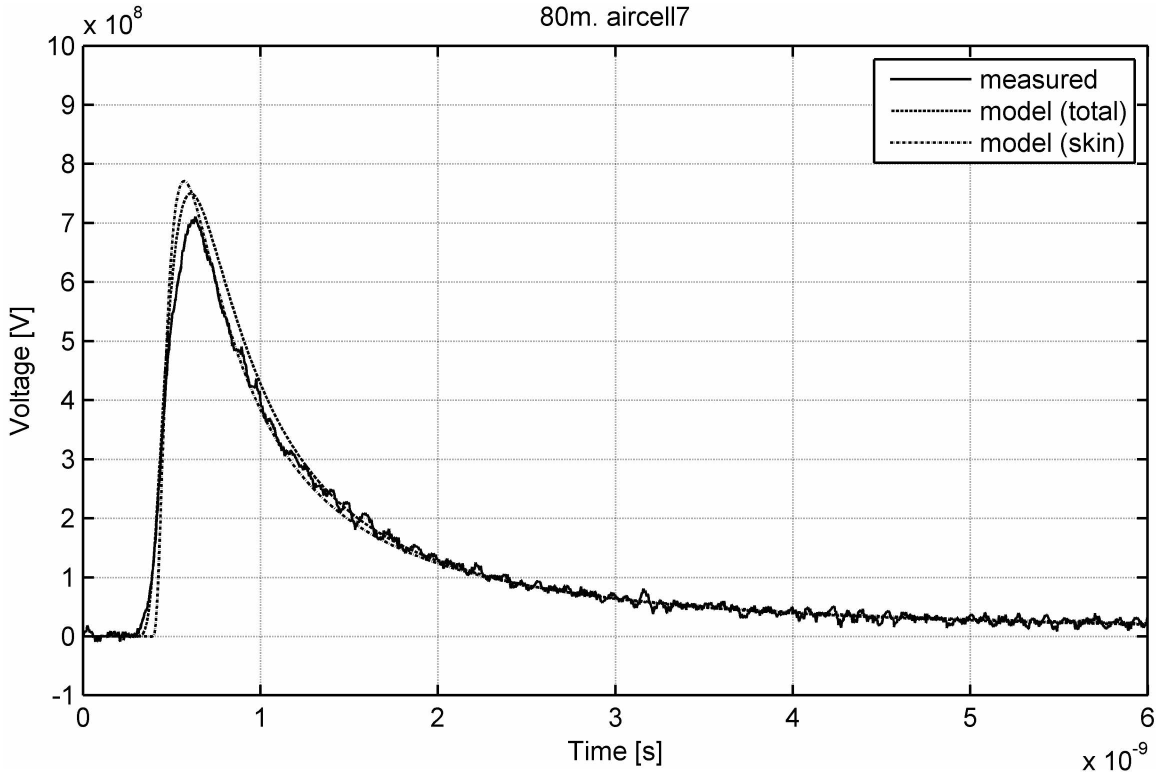

Fig. 19. Impulse response from measurements and model fit for 80m Aircell7 cable (c).

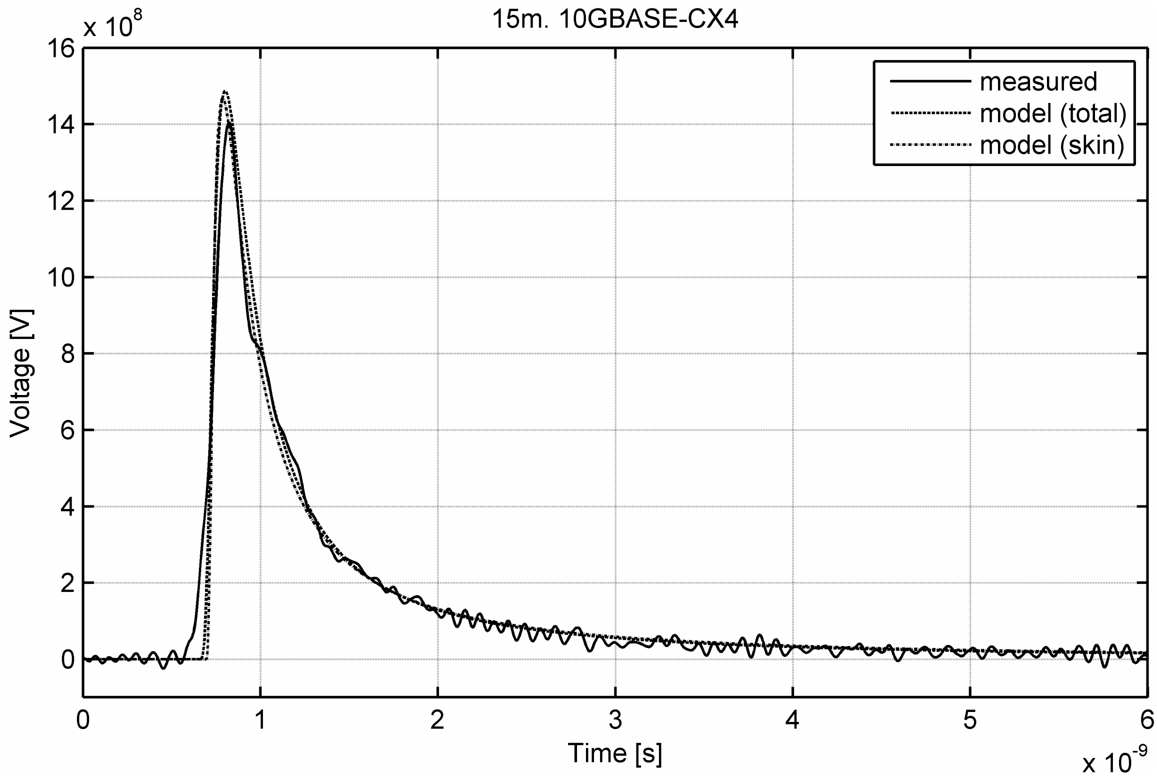

Fig. 20. (Differential) impulse response from measurements and model fit for 15m 10GBASE-CX4 24AWG (d).

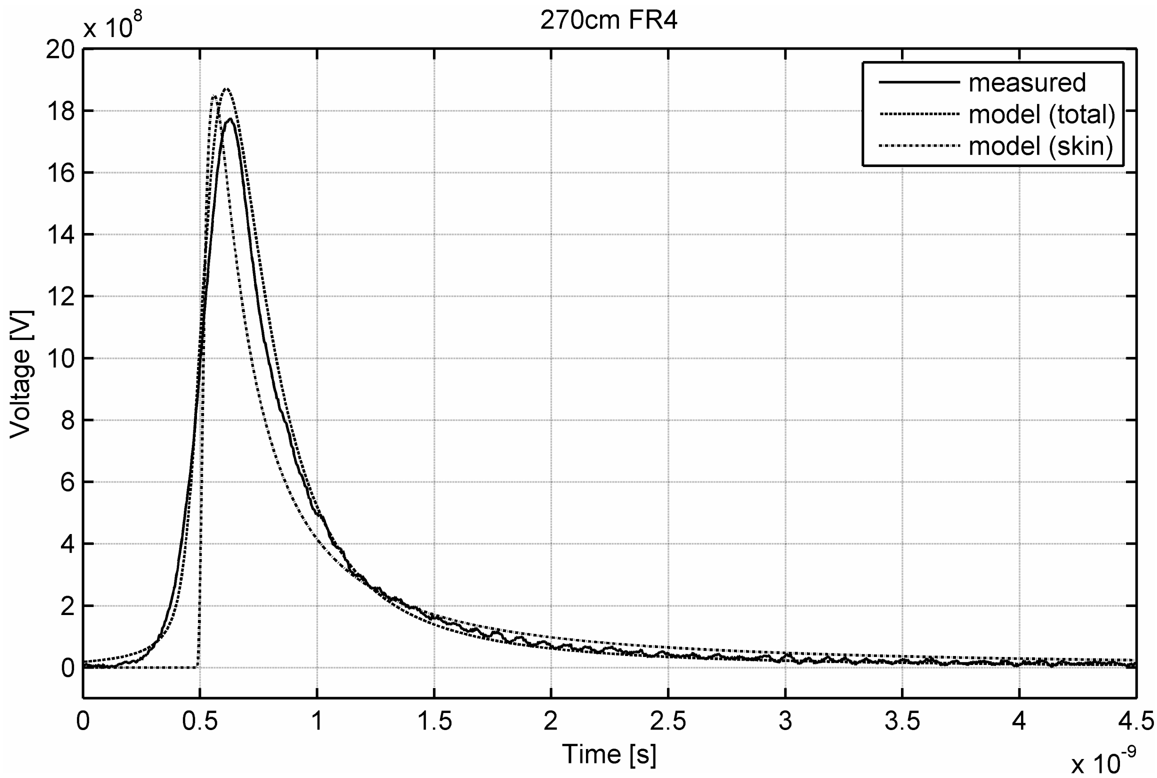

Fig. 21. Impulse response from measurements and model fit for 270cm long microstrip on FR4 printed circuit board (e).

2.6. Conclusions

A practical model for copper channels is described, modeling both skin effect and dielectric loss. Special attention was given to causality, to provide an accurate impulse response for use in high speed transient simulations.

The well known formulas for skin effect were combined with a new formula for dielectric loss in FR4, published only in 2001. This formula for dielectric loss is shown in this chapter to be not only useful and accurate for modeling the dielectric loss on printed circuit boards, but also for modeling cables. Both the complex skin-effect impedance and the complex dielectric impedance comply with the Kramers-Kronig relations. Therefore, an inverse Fourier transform of the transfer function yields a causal time domain response.

Measurements show a good model fit in the time domain with coaxial copper cables, a twisted pair cable, and a printed circuit board trace. We can conveniently use the modeled impulse response for accurate transient simulations of high-speed communication systems.